ChemistrySelect

Research Article
doi.org/10.1002/slct.202402379

Chemistry Europe
European Chemical Societies Publishing

www.chemistryselect.org

Network Pharmacology Integrated With Quantum-Polarized Ligand Docking and Molecular Simulation Revealed the Anti-Diabetic Potential of Curcumin

Abbas Khan,*[a] Abrar Mohammad Sayaf,[b] AbdalRahman Alshammarri,[c] Muhammad Ammar Zahid,[a] Raed M. Al-Zoubi,[d, e, f] Mohanad Shkoor,[g] Tarek Benameur,[h] Dong-Qing Wei,[j] and Abdelali Agouni*[a, i]

Diabetes mellitus is a chronic metabolic disorder affecting millions of people worldwide and causes serious complications such as diabetic nephropathy. Curcumin, a natural polyphenol derived from turmeric, has demonstrated antidiabetic, anti-inflammatory, and antioxidant properties. However, the molecular mechanisms underlying curcumin's anti-diabetic effects remain incompletely understood. This study employed network pharmacology, molecular docking, and simulation techniques to explore the potential targets, and key pathways of curcumin in the treatment of diabetes. Using SwissTarget prediction and Superpred databases, we predicted the molecular targets for curcumin, while diabetes-associated genes were obtained from DisGeNet. We identified 60 common targets for curcumin in diabetes. Protein-protein interaction (PPI) analysis revealed three sub-networks and ten hub genes with AKT1, TNF-α, EGFR, and STAT3 identified as key hub genes that could serve as potential biomarkers. Gene enrichment analysis indicated that these genes primarily regulate insulin resistance and other metabolic pathways. Quantum-polarized ligand docking (QPLD) showed that curcumin establishes multiple hydrogen and hydrophobic interactions with the essential amino acids of these hub targets. Molecular simulation results demonstrated stable dynamic behavior, a compact structure, and variations in residue flexibility. Binding free energy calculations using MM/GBSA and MM/PBSA methods validate curcumin's strong binding to the potential targets. Total binding free energy using MM/GBSA ranged from −21.35 to −30.94 kcal/mol while MM/PBSA calculations showed total binding free energy values between −19.80 and −26.66 kcal/mol. Altogether, this study provides valuable insights into the molecular targets of curcumin in diabetes and lays the foundation for future advancements in diabetes treatment.

1. Introduction

Diabetes is a chronic metabolic disorder affecting millions globally and ranks as the seventh leading cause of death in the United States.[1] The primary characteristic of diabetes is the body's inability to regulate blood glucose levels, either due to insufficient insulin production or ineffective insulin action, a hormone that facilitates glucose uptake by cells.[2] Common symptoms of diabetes include increased thirst, frequent urination, hunger, fatigue, blurred vision, and slow wound healing.[3]

[a] A. Khan, M. A. Zahid, A. Agouni
Department of Pharmaceutical Sciences, College of Pharmacy, QU Health, Qatar University, Doha P.O. Box 2713, Qatar
E-mail: Abbaskhan@sjtu.edu.cn
aagouni@qu.edu.qa

[b] A. M. Sayaf
School of Chemical Sciences, Universiti Sains Malaysia, Penang 11800, Malaysia

[c] A. Alshammarri
Department of Pharmacology and Toxicology, College of Pharmacy, King Saud University, Post Box 2455, Riyadh 11451, Saudi Arabia

[d] R. M. Al-Zoubi
Surgical Research Section, Department of Surgery, Hamad Medical Corporation, Doha, Qatar

[e] R. M. Al-Zoubi
Department of Biomedical Sciences, College of Health Sciences, QU Health, Qatar University, Doha P.O. Box 2713, Qatar

[f] R. M. Al-Zoubi
Department of Chemistry, Jordan University of Science and Technology, P.O. Box 3030, Irbid 22110, Jordan

[g] M. Shkoor
Department of Chemistry, College of Arts and Science, Qatar University, P.O. Box 2713, Doha, Qatar

[h] T. Benameur
College of Medicine, King Faisal University, PO Box 400, Al-Ahsa, Kingdom of Saudi Arabia

[i] A. Agouni
Office of Vice President for Research and Graduate Studies, Qatar University, Doha, Qatar

[j] D.-Q. Wei
Department of Bioinformatics and Biostatistics, College of Life Sciences and Biotechnology, Shanghai Jiao Tong University, Shanghai, P. R. China

According to the World Health Organization (WHO), the number of diabetes cases increased from 108 million in 1980 to 422 million in 2014.[4] The prevalence of diabetes has been rising more rapidly in low- and middle-income countries compared to high-income countries.[4] In 2019, an estimated 463 million adults worldwide had diabetes, with projections indicating this number could reach 700 million by 2045.[5] Diabetes was responsible for 4.2 million deaths and $374 billion in health expenditures in 2019. The most prevalent form of diabetes is type 2 diabetes, which accounts for 90–95% of all cases, and is largely associated with modifiable risk factors such as obesity, physical inactivity, and unhealthy diet.[6] Additionally, diabetes caused 460,000 kidney disease deaths and contributed to around 20% of cardiovascular deaths due to elevated blood glucose levels.[7]

The management of diabetes necessitates a comprehensive strategy that encompasses lifestyle modifications, pharmacological interventions, and regular monitoring of blood glucose and other health parameters. The primary objectives of diabetes treatment are to prevent both acute and chronic complications, enhance quality of life, and reduce mortality.[8] Lifestyle interventions, including dietary counselling, physical activity, weight management, and smoking cessation, are fundamental to diabetes care and can prevent or delay the onset of type 2 diabetes in individuals at high risk.[9] Pharmacological interventions include various classes of drugs that act on different targets to lower blood glucose levels, such as insulin, metformin, sulfonylureas, glucagon-like peptide (GLP)-1 receptor agonists, sodium-glucose cotransporter-2 (SGLT2) inhibitors, and dipeptidyl peptidase-4 (DPP-4) inhibitors. The selection of drug depends on the type and severity of diabetes, as well as the patient's characteristics, preferences, and comorbidities.[10] Regular monitoring of blood glucose and other parameters, such as blood pressure, lipid profile, kidney function, and eye health, is essential to assess the treatment effectiveness, identify complications, and adjust therapy as needed.[11] Despite its challenges, medication remains a vital treatment option in the field of endocrinology and is likely to maintain its significance for an extended period. Consequently, innovative therapeutic approaches utilizing advanced techniques are essential for discovering more effective alternative treatments.[12]

The conventional approach to drug discovery, which focuses on a single drug, target and disease, faces challenges in safety, efficacy, and sustainability. Network pharmacology, an emerging paradigm, integrates network biology and polypharmacology to address these limitations.[13] This approach leverages computational tools to map molecular interactions of drug candidates within cellular network and assess their effects on both the interactome and the diseasome.[14] Network pharmacology facilitates the discovery of novel drug leads, targets, and indications, while optimizing the safety and efficacy of existing drugs by exploiting the complex relationships between natural products and the human body.[15] This strategy offers a promising solution to drug development challenges in the era of omics data and systems biology.[13]

Curcumin, a natural compound derived from the rhizome of the plant Curcuma longa (turmeric) has been used in traditional medicine for centuries due to its anti-inflammatory, antioxidant, anticancer, neuroprotective, and anti-diabetic properties.[15,16] It can modulate multiple targets and pathways involved in glucose metabolism, insulin signalling, inflammation, oxidative stress, and apoptosis.[17] Additionally, curcumin can enhance the effects of existing antidiabetic drugs, such as metformin, sulfonylureas, and thiazolidinediones. However, curcumin has limitations, including low bioavailability, poor solubility, and rapid metabolism.[18,19] Therefore, it is essential to improve its pharmacokinetic and pharmacodynamic properties and to identify optimal dosage and drug combinations.[18] Importantly, the molecular targets of curcumin in diabetes are not yet fully elucidated. Identifying these targets will enhance our understanding of the cellular pathways underlying curcumin's anti-diabetic actions and reveal novel molecular targets for diabetes treatment.

Given curcumin's anti-diabetic potential, the present study employs network pharmacology combined with QPLD and molecular simulation to discover novel targets for curcumin. Furthermore, binding free energy is calculated for the top hub genes-curcumin complexes. This research aims to guide the selective inhibition of diabetes targets in clinical trials.

2. Material and Methods

2.1. Target Prediction for Curcumin

We utilized two databases to identify potential targets for curcumin: SwissTarget Prediction (http://www.swisstargetprediction.ch/)[20] and Superpred (https://prediction.charite.de/)[21] Additionally, we searched for "diabetes" in DisGeNet to obtain diabetes-related proteins/genes. We then compared the predicted targets with the diabetes-related genes and selected the common ones for the PPI network construction. Figure 1 illustrates the methodological workflow of our study.

2.2. Construction of the PPI Network

We employed the STRING database (https://string-db.org/cgi/input?sessionId = btWeOUvPdvTt&input_page_active_form = multiple_identifiers) to construct the PPI network for curcumin's potential targets against diabetes using the highest confidence level (0.900) as the parameter.[22,23] We then imported the PPI network into Cytoscape v3.8.2 to identify the subnetworks and screen core targets. The Molecular Complex Detection (MCODE) algorithm based plugin was used with specific parameters: Degree Cutoff = 2, Node Score Cutoff = 0.2, and K-Core = 2. We subsequently selected the top 4 core targets based on Cytohubba analysis.[24–26]

2.3. Structural Retrieval and QLPD

We obtained the crystallographic coordinates of the proteins from the RCSB Protein Data Bank. For proteins lacking avail-

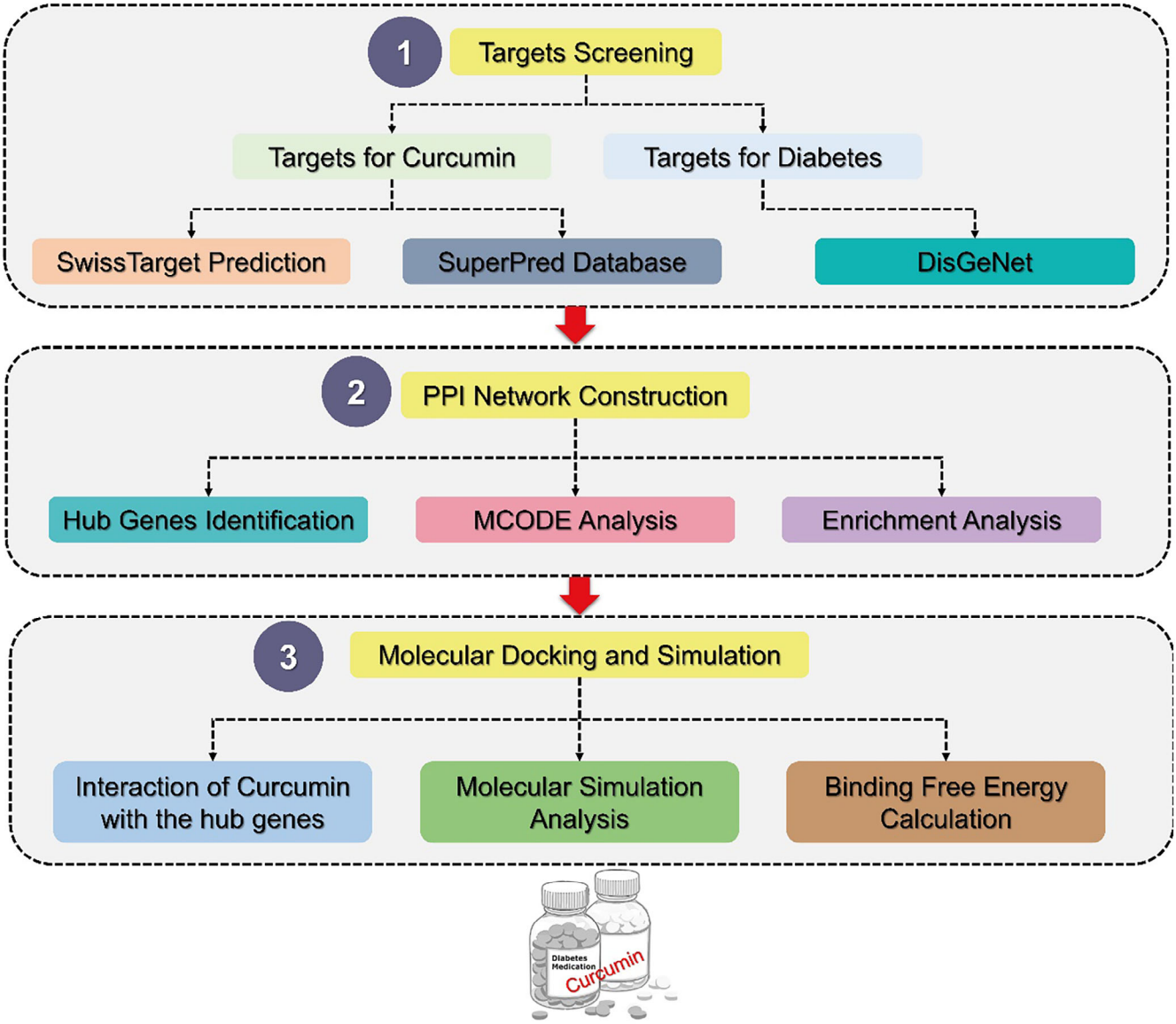

Figure 1. Systematic workflow of the study. The first step involves retreiving and predicting targets for curcumin and diabetes. Then PPI was constructed and small subnetworks along with the hub genes were identified. Finally, molecular docking of curcumin with the key hub genes and simulation was performed.

able coordinates, we utilized AlphaFold 2.0 to model their structures, as referenced in previous studies.[27,28] The protein structures were then prepared using the Protein Preparation Wizard in Schrodinger Maestro, applying default settings for pre-processing. The refinement was conducted at a pH of 7.0 using the OPLS 2.1 force field.[29] A restrained minimization was performed until the root mean square deviation (RMSD) of the heavy atoms converged to 0.30 Å. The ligand molecule, identified as CID 969 516, was downloaded from PubChem and subsequently minimized using the MMFFx force field. The binding site of the protein was detected using the Sitemap module. To further investigate the ligand-protein interactions, we employed advanced docking methods, including scoring functions, to estimate binding energies and provide quantitative insights into these interactions.[30] To evaluate curcumin's activity against selected targets, we utilized the QPLD approach. This method integrates quantum mechanical and molecular mechanics properties to offer a more accurate assessment of small molecule binding potential.[31] Compared to traditional docking methods, QPLD provides a more precise description of electronic interactions between the ligand and protein by accounting for polarization effects due to charge distribution. The QPLD approach employs density functional theory (DFT) or semi-empirical methods to quantify the properties of both the protein and ligand. In our study, we applied QPLD with a ligand vdW scaling factor of 0.8, an RMSD deviation threshold of less than 0.5, and allowed a maximum of 10 poses using Schrodinger Maestro software. Jaguar was used for assigning QM charges, and extra precision (XP) approaches were employed for re-docking, with a maximum atomic displacement of 1.3 Å. The best pose was visualized using PyMOL for detailed molecular interaction analysis.[32]

2.4. All-Atoms Simulation in Explicit Solvent

The molecular simulations for all systems were prepared using the "tLeap" module in AMBER21.[33,34] Each system was solvated in an optimal point charge (OPC) solvent box, with ions added to neutralize the charge. The ligand molecule was parameterized using the GAFF2 force field, with initial topology and force field modification (frcmod) files generated using antechamber and parmchk2. Energy minimization was performed on each system using steepest descent and conjugate gradient algorithms until convergence, based on a defined maximum force or energy change threshold. To achieve the desired simulation temperature and equilibrate the system, a temperature coupling algorithm (such as Langevin Dynamics or Berendsen thermostat) was employed to gradually heat the system from a low temperature. Long-range electrostatic interactions were computed using the Particle Mesh Ewald (PME) method, while van der Waals forces were determined using Lennard-Jones potential.[35] The systems were equilibrated at the target temperature and pressure through stages involving positional restraint, slow heating, and unrestrained equilibration. The SHAKE algorithm was used to constrain covalent bond lengths and angles, and system pressure was controlled using a barostat such as Berendsen or Andersen.[36] Following equilibration, each system underwent a 300 ns production simulation using a molecular dynamics algorithm such as NPT or NVT ensemble.[37] Simulation parameters, including time step and cut-off distances, were set during this step. The trajectory from the production run was analyzed using CPPTRAJ or PTRAJ modules.[38] This analysis encompassed the calculation of root mean square deviation (RMSD), root mean square fluctuation (RMSF), radius of gyration (Rg), and hydrogen bonding for each system.[39–41]

2.5. Binding free Energy Estimation Through MM/GBSA and MM/PBSA Analysis

We employed both MM/GBSA and MM/PBSA approaches to calculate binding free energies (BFE) for protein-ligand complexes. These methods offer a balance between computational efficiency and accuracy for assessing binding affinities. We calculated the BFE for each complex ($G_{(complex,\ solvated)}$) and the unbound states of curcumin ($G_{(curcumin,\ solvated)}$) and receptors ($G_{(receptors,\ solvated)}$). The following equation was used to calculate each term in the total binding energy:

$$\Delta G_{bind} = G_{(complex,\ solvated)} - G_{(curcumin,\ solvated)} - G_{(receptors,\ solvated)} \quad (1)$$

where:

$$G = E_{Molecular\ Mechanics} - G_{solvated} - TS \quad (2)$$

The binding energy components were:

$$\Delta G_{bind} = \Delta E_{Molecular\ Mechanics} + \Delta G_{solvated} - \Delta TS = \Delta G_{vaccum} + \Delta G_{solvated} \quad (3)$$

$$\Delta E_{Molecular\ Mechanics} = \Delta E_{int} + \Delta E_{electrostatic} + \Delta E_{vdW} \quad (4)$$

$$\Delta\ G_{solvated} = \Delta G_{Generalized\ born} + \Delta G_{surface\ area} \quad (5)$$

MM/GBSA uses the Generalized Born model for ΔGsolvated, while MM/PBSA employs the Poisson-Boltzmann equation. Both methods calculate nonpolar solvation energy (ΔGsurface area) using a linear function of solvent-accessible surface area (SASA):[42]

$$\Delta\ G_{surface\ area} = \gamma .SASA + b \quad (6)$$

Conformational entropy was not calculated due to computational limitations. ΔEinternal was zero in single trajectory calculations.[43]

3. Results and Discussion

3.1. Target Retrieval and Protein Network Construction

Curcumin (1,7-bis(4-hydroxy-3-methoxyphenyl-)-1,6-heptadiene-3,5-dione), also known as diferuloylmethane, is a polyphenol found in Curcuma species.[44] This compound has shown promising therapeutic potential due to its anti-inflammatory, anti-diabetic, anti-cancer, and antioxidant properties. Research suggests that curcumin may have applications in treating various conditions, including arthritis, cancer, and neurodegenerative diseases, although further studies are necessary to establish its clinical efficacy.[45] Given curcumin's broad pharmacological applications, we utilized it to identify novel therapeutic targets in diabetes. Using SwissTarget, 100 targets were predicted, of which 54 overlapped with the therapeutic targets listed in DisGeNet. Additionally, Superpred predicted 9 targets for curcumin, with 6 of these targets also appearing in the DisGeNet list. The 2D structure of curcumin is shown in Figure 2a, while Figure 2b presents a Venn diagram depicting the overlap of predicted targets. The 60 overlapping proteins were subsequently used to construct a PPI network, as shown in Figure 2c.

3.2. Identification of Sub-Networks and Hub Genes

In PPI networks, small subnetworks play a crucial role in understanding localized cellular processes and activities. Identifying these subnetworks contributes to the discovery of specific protein clusters, which aids in identifying potential drug targets and provides insights into disease mechanisms.[46,47] These findings have potential applications in personalized medicine and tailored treatments. Considering the importance of subnetworks in disease management, we employed MCODE to detect the small subnetworks in the large PPI network. Three small subnetworks were identified. The first subnetwork comprised 20 targets, with AKT1 and TNF-α as key nodes (Figure 3a). The second subnetwork consisted of 9 targets, with EGFR, HSPA1N, and HSP90AB1 as primary nodes (Figure 3b). The third subnetwork contained 6 targets, with STAT3 as a major hub gene (Figure 3c).

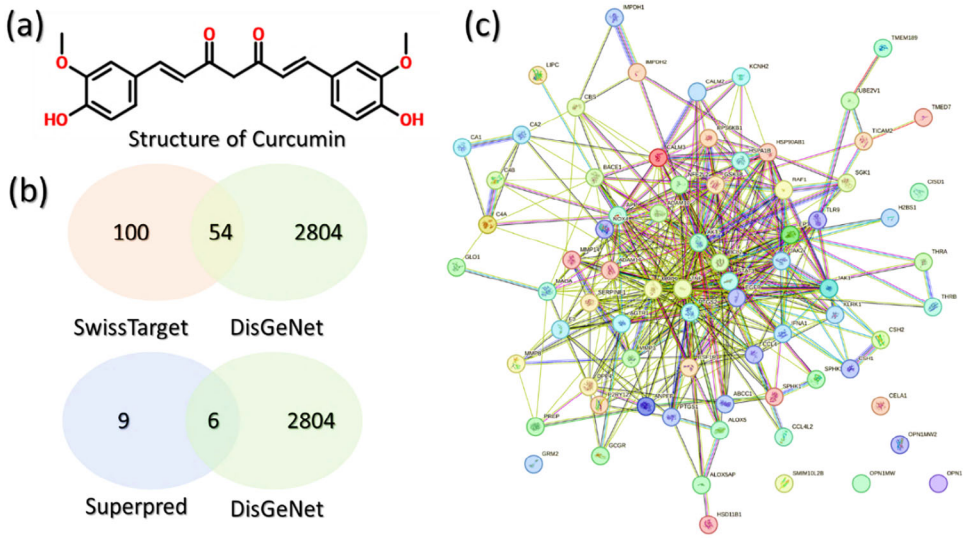

Figure 2. Curcumin predicted targets and the PPI network. Panel (a) shows the 2D structure of curcumin, panel (b) shows the Venn diagram for the SwissTarget and Superpred with the DisGeNet list, and panel (c) shows the PPI network of the common targets constructed by using the STRING database.

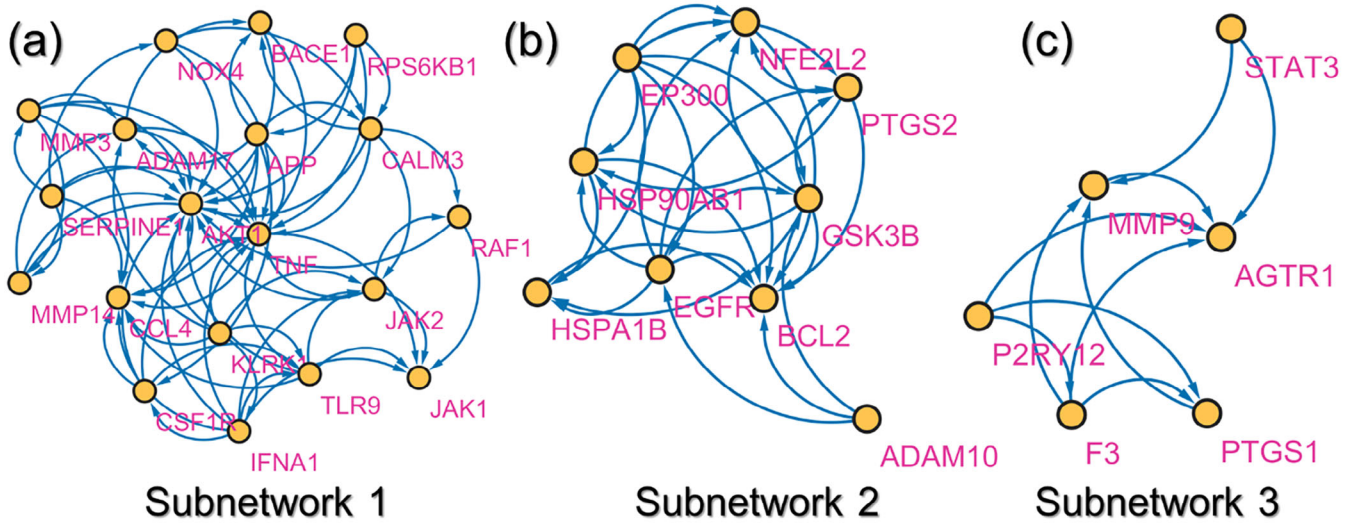

Figure 3. Identification of small sub-networks in the whole PPI network. a) Subnetwork 1 with 20 targets, b) Subnetwork 2 with 9 proteins, and c) Subnetwork 3 with 6 proteins.

Furthermore, we identified hub genes in the entire PPI network that may serve as novel biomarkers for the treatment of diabetes. Hub genes are pivotal regulators orchestrating diverse cellular functions within biological networks. Their importance lies in being fundamental elements that, when targeted, can disrupt disease-associated processes. A comprehensive understanding of hub gene involvement is essential for advancement of therapeutic strategies. The identification and manipulation of hub genes, which are crucial molecular actors in pathological processes, represent promising avenues for the precision medicine, facilitating the development of tailored pharmacotherapies for various disorders.[48] Based on degree centrality, our analysis predicted 10 targets as hub genes. TNF-α emerged as the top biomarker with a degree score of 48, followed by AKT1 (43), EGFR (36), STAT3 (35), BCL2 (34), MMP9 (32), PTGS2 (31), APP (26), GSK3B (23), and CALM3 (21). These hub genes are potential targets for curcumin in diabetes treatment. Figure 4a displays the identified hub genes in red, orange, and yellow based on their degree score in the PPI network, while Figure 4b shows the ranking of the hub genes. Our findings align with previous reports where these targets, particularly TNF-α, AKT1, STAT3, and EGFR have been identified as important for the treatment of diabetes.[49–52] This suggests that targeting these molecules with curcumin could produce a positive pharmacological outcome and alleviate the burden of diabetes.

3.3. Transcription factor identification in the gene regulatory network

In this analysis, we identified the key transcription factors (TFs) and protein kinases linked to differentially expressed genes

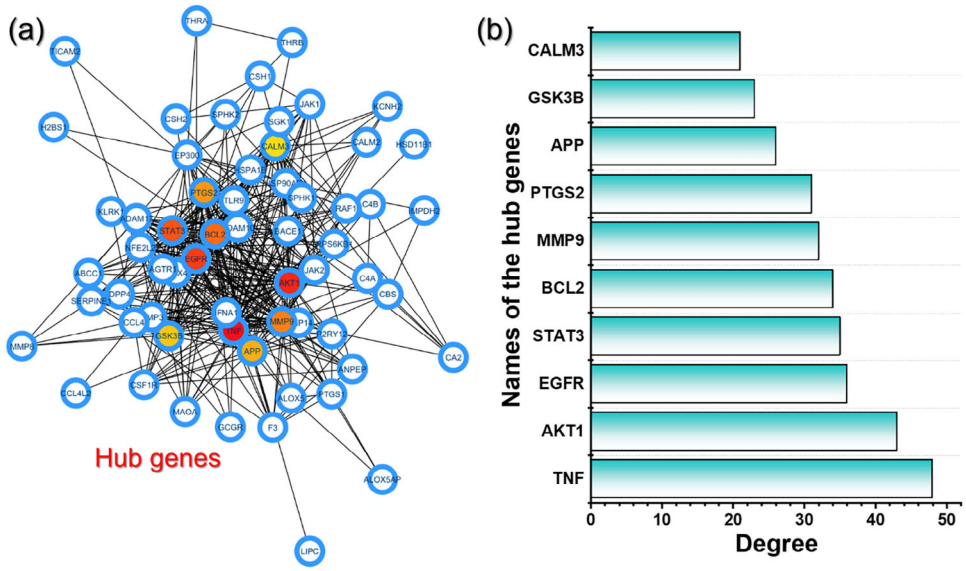

Figure 4. Identification and ranking of the hub genes in the PPI network based on the degree property. Panel (a) shows the hub genes (red, orange, and yellow) in the whole PPI while panel (b) shows the degree scores for each hub gene in the PPI.

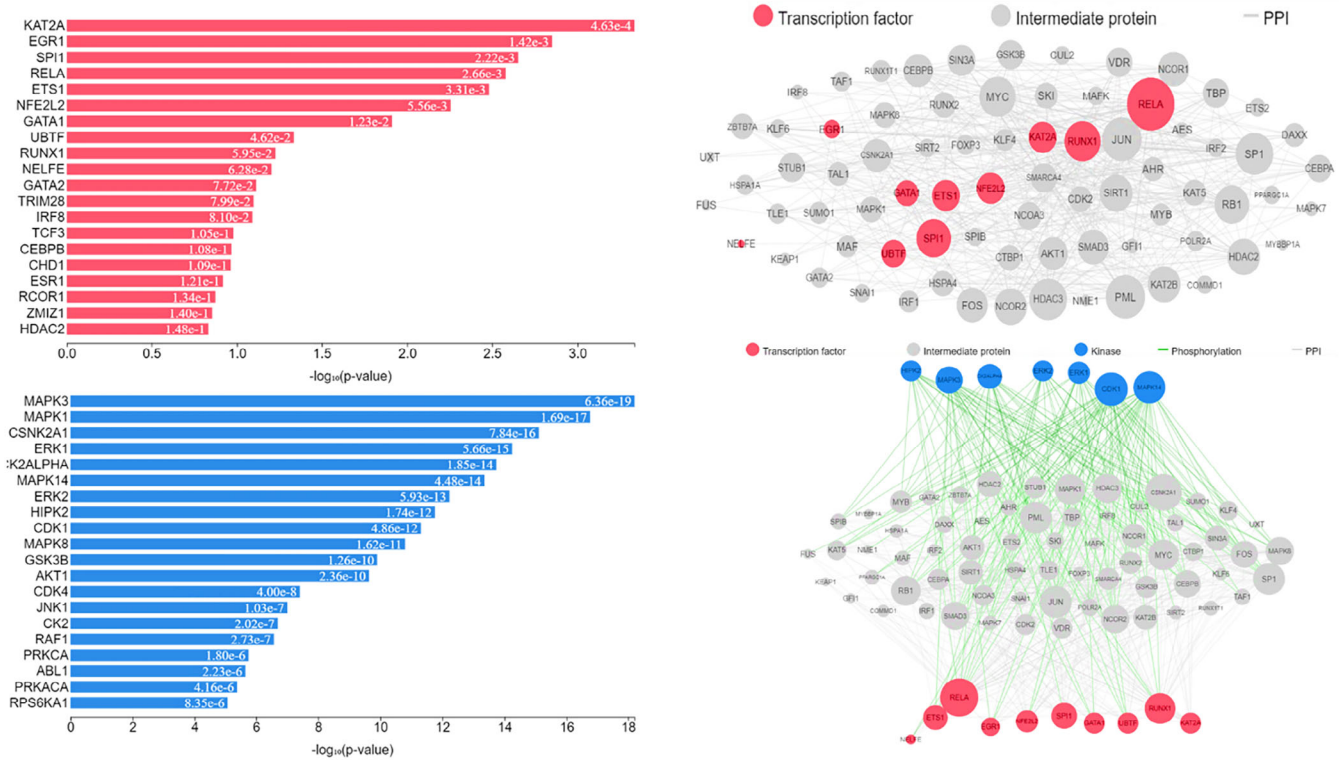

Figure 5. Prediction of TFs and specific kinases that regulate the constructed PPI using ChIP-seq experiments (ChEA) based on the hypergeometric p-value. (a-b) shows the predicted top TFs that are interconnected to other nodes to regulate the PPI network while (c-d) shows the specific kinases that perform the regulatory function. TFs, transcription factors.

based on their roles in regulatory network progression. The regulatory network was constructed by connecting TFs, kinases, and their associated transient proteins, which are involved in forming the regulatory complex. Initially, we used ChIP-seq experiments (ChEA) to determine the integrated target genes for transcription factors. This approach allowed us to predict the most significant TFs, which were then mapped onto the PPI network. The predicted TFs and the PPI network are illustrated in Figure 5a,b. The top TFs include RELA, RUNX1, KAT2A, NFE2L2, ETS1, GATA1, SPI1, UBTF, EGR1, and NEFE based on the hypergeometric *p*-value. Kinases that are likely the regulators of the expanded PPI network were also identified and mapped on the PPI network. Figure 5c,d, show the top predicted kinases and their PPI network. Based on the hypergeometric *p*-value, MAPK14,

CK2ALPHA, CDK1, ERK2, ERK1, HIPK2, and MAPK3 were found to be the topmost kinases in these differentially expressed genes. Interestingly, these TFs are reported in experimental setups to be associated with pathways upregulated in diabetes.[53] For instance, RELA has been reported to govern a network of islet-specific metabolic genes necessary for beta cell function.[54] Moreover, specific kinases such as CDK1 are reported to be associated with the metabolic pathways that are associated with diabetes.[55,56] Hence, this shows the validity of our findings related to the specific TFs and kinases that regulate this PPI network.

3.4. Enrichment Analysis of the PPI Network

Enrichment analysis in PPI networks is vital for elucidating the biological relevance of identified protein clusters. By assessing functional annotations and pathway associations within these clusters, enrichment analysis helps uncover the underlying biological processes. This not only enhances our understanding of complex cellular mechanisms but also provides critical insights for prioritizing potential therapeutic targets and guiding experimental efforts in drug development, ultimately contributing to more effective and targeted interventions against various diseases.[57] We determined the role of each protein in the diabetes pathways and their biological and molecular function in this disease. TNF-α and AKT1 were reported to be involved in insulin signaling and resistance pathways. Moreover, the factors and pathways affecting insulin-like growth factor 1 (IGF1)-AKT1 signaling were also significant in these selected genes. The other proteins such as APP were observed to be associated with regulation of reactive oxygen species metabolic process biological process. Our findings are validated by previous literature where TNF-α and AKT1 have been reported to be essential in these pathways. For instance, it has been reported that targeting TNF-α is an effective strategy for the treatment of insulin resistance and type 2 diabetes.[52] Table 1 summarizes the significant pathways, biological processes, and molecular functions of these proteins in the whole PPI network.

3.5. Molecular Docking of the Key Hub Genes With Curcumin

To investigate the interaction pattern of curcumin with the key hub genes, we used a molecular docking approach to determine the binding pattern with AKT1, TNF-α, STAT3, and EGFR. Using the QPLD approach, the molecular interaction pattern was determined. The interaction patterns of the curcumin with AKT1 and TNF-α are shown in Figure 6,b. It can be observed that curcumin established several hydrogen bonds and other interactions with AKT1. Among the hydrogen bonds Glu191, Thr195, Thr211, and Glu228 residues are involved. The other interactions involve Phe161, Val164, Ala177, Leu181, Met227 and Met281. This shows a robust interaction of curcumin with AKT1 and consequently produces desirable pharmacological properties. On the other hand, the curcumin-bound TNF-α complex reported two hydrogen bonding interactions and two hydrophobic interactions including the residues Gly121, Tyr151, Tyr59, and Ala96. The hypoglycemic effects of curcumin involve multiple mechanisms, including the reduction of plasma-free fatty acids (FFAs) and TNF-α levels.[58,59] This shows that our predicted targets are well characterized in diabetes and that the effect of curcumin strongly aligns with our findings.

Moreover, the interaction pattern of curcumin with STAT3 and EGFR was also calculated to determine the binding potential and further decipher the pharmacological properties of curcumin. As depicted in Figure 7a,b, curcumin established several interactions with STAT3 and EGFR. Several hydrogen bonds involving Lys728, Lys745, Met793, and Asp855 from EGFR are involved in interactions with curcumin while residues Leu718, Val726, Lys728, Leu788, Met790, and Leu1001 are involved in interactions other than hydrogen bonding. The interaction pattern of curcumin with STAT3 also revealed several hydrogen bonds such as Ser611, Glu612, Ser613, Gln635, Ser636 and Glu638. Moreover, Arg609, Phe610, Val637, and Pro639 are involved in non-hydrogen bonding interactions. Overall, these findings show that curcumin robustly interacts with these targets and consequently produces desirable pharmacological properties in diabetes.

3.6. Molecular Simulation-Based Dynamic Stability Assessment

To quantify the structural stability during simulation we performed root mean square deviation (RMSD) analysis of each complex to determine the binding stability using the simulation trajectories. As shown in Figure 8a, the curcumin-AKT1 complex stabilized at 1.65 Å and maintained a similar level throughout the simulation with a minor perturbation at 160 ns where a decrease in the RMSD level was observed. The RMSD stabilized completely after 160 ns with no further perturbation. The curcumin-TNF-α complex shown in Figure 8b, was the most stable complex during the simulation. An average RMSD was reported to be 2.0 Å with no significant structural perturbation. The RMSD continued to increase and stabilized at 2.0 Å and maintained the same level until the end of the simulation. This shows the structural stability of the curcumin when bound to TNF-α. Unlike these two complexes, the EGFR-curcumin complex reported significant deviations in the RMSD pattern and maintained a similar behavior throughout the simulation. The RMSD level reached up to 4.0 Å and thus shows that this complex remained unstable during the simulation. The RMSD graph for curcumin-EGFR is shown in Figure 8c. The curcumin-STAT3 complex also demonstrated a stable and uniform RMSD pattern until 100 ns and then an abrupt increase was observed; however, the structure stabilized and maintained a steady level of RMSD till the end of the simulation. An average RMSD for the curcumin-STAT3 complex was calculated to be 1.8 Å. The RMSD graph for the curcumin-STAT3 complex is shown in Figure 8d. In sum, these results show that the binding of curcumin to these targets is stable and therefore determines to maintain a better pharmacological potential against these targets in diabetes.

Table 1. Enrichment analysis of the PPI network. The WikiPathways, KEGG pathways, GO biological process and molecular functions are provided.

# Genes	Category	Description	FDR Value	Genes
3	WikiPathways	Role of ceramides in the development of insulin resistance	$4.90E^{-05}$	RPS6KB1, TNF-α, AKT1
4	KEGG Pathways	Insulin signaling pathway	$9.64E^{-05}$	RPS6KB1, CALM3, RAF1, AKT1
3	KEGG Pathways	Insulin resistance	$9.00E^{-04}$	RPS6KB1, TNF-α, AKT1
2	WikiPathways	Leptin-insulin signaling overlap	0.0019	JAK2, AKT1
3	WikiPathways	Insulin signaling	0.0045	RPS6KB1, RAF1, AKT1
2	WikiPathways	Factors and pathways affecting insulin-like growth factor (IGF1)-AKT1 signaling	0.0052	RPS6KB1, AKT1
15	GO Biological Process	Regulation of nitrogen compound metabolic process	$7.60E^{-04}$	SERPINE1, RPS6KB1, KLRK1, NOX4, IFNA1, APP, CSF1R, CALM3, MMP14, ADAM17, TLR9, JAK2, TNF-α, RAF1, AKT1
16	GO Biological Process	Regulation of metabolic process	$8.70E^{-04}$	SERPINE1, RPS6KB1, KLRK1, NOX4, IFNA1, APP, CSF1R, CALM3, MMP3, MMP14, ADAM17, TLR9, JAK2, TNF-α, RAF1, AKT1
17	GO Biological Process	Metabolic process	0.001	SERPINE1, RPS6KB1, KLRK1, NOX4, APP, CSF1R, CALM3, MMP3, MMP14, ADAM17, BACE1, TLR9, JAK2, TNF-α, RAF1, AKT1, JAK1
12	GO Biological Process	Protein metabolic process	0.0027	RPS6KB1, APP, CSF1R, MMP3, MMP14, ADAM17, BACE1, TLR9, JAK2, RAF1, AKT1, JAK1
14	GO Biological Process	Regulation of cellular metabolic process	0.0037	RPS6KB1, KLRK1, NOX4, IFNA1, APP, CSF1R, CALM3, MMP3, ADAM17, TLR9, JAK2, TNF-α, RAF1, AKT1
14	GO Biological Process	Macromolecule metabolic process	0.0044	RPS6KB1, NOX4, APP, CSF1R, MMP3, MMP14, ADAM17, BACE1, TLR9, JAK2, TNF-α, RAF1, AKT1, JAK1
13	GO Biological Process	Organonitrogen compound metabolic process	0.0048	RPS6KB1, NOX4, APP, CSF1R, MMP3, MMP14, ADAM17, BACE1, TLR9, JAK2, RAF1, AKT1, JAK1
6	GO Biological Process	Negative regulation of protein metabolic process	0.0129	SERPINE1, APP, CALM3, TNF-α, RAF1, AKT1
3	GO Biological Process	Regulation of reactive oxygen species metabolic process	0.0137	APP, MMP3, TNF-α
3	GO Biological Process	Positive regulation of small molecule metabolic process	0.0145	APP, TNF-α, AKT1
14	GO Biological Process	Nitrogen compound metabolic process	0.016	RPS6KB1, KLRK1, NOX4, APP, CSF1R, MMP3, MMP14, ADAM17, BACE1, TLR9, JAK2, RAF1, AKT1, JAK1

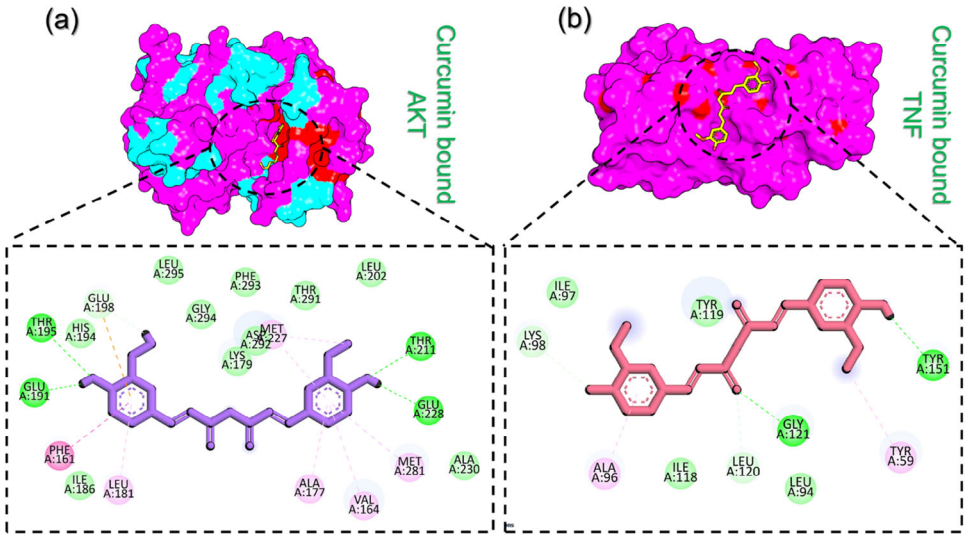

Figure 6. Molecular docking analysis of curcumin with AKT1 and TNF-α. Panel (a) shows the binding pattern of curcumin with AKT1 and the 2D interaction patterns while panel (c) shows the binding pattern of curcumin with TNF-α and the 2D interaction pattern.

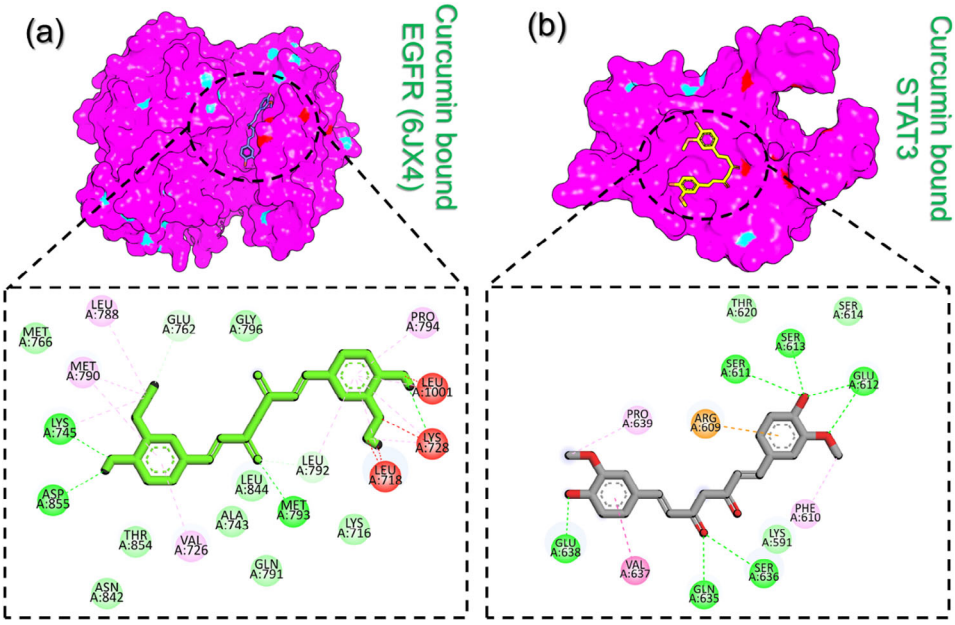

Figure 7. Molecular docking analysis of curcumin with EGFR and STAT3. Panel (a) shows the binding pattern of curcumin with EGFR and the 2D interaction patterns while panel (c) shows the binding pattern of curcumin with STAT3 and the 2D interaction pattern.

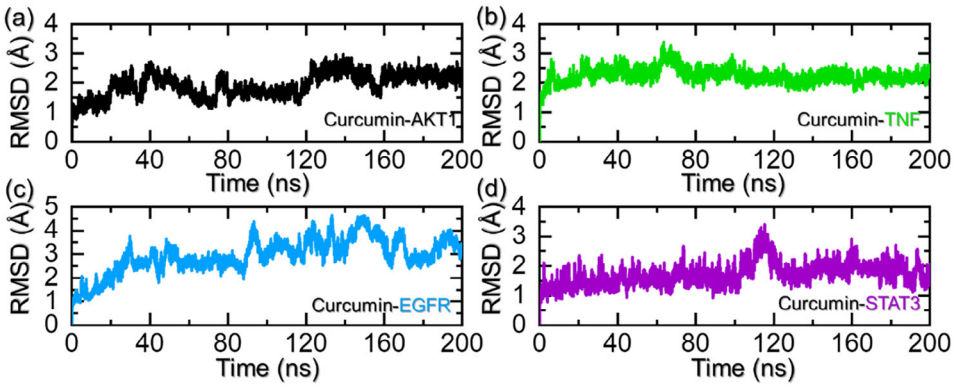

Figure 8. Dynamic stability analysis of the curcumin-bound complexes. Panel (a) shows the RMSD graph for curcumin-AKT1 complex, panel (b) shows the RMSD graph for the curcumin-TNF-α complex, panel (c) shows the RMSD graph for the curcumin-EGFR while (d) shows the RMSD graph for the curcumin-STAT3 complex.

3.7. Structural Compactness Analysis

Structural compactness assessment through Rg calculation is among the key parameters that can be used to harness the pharmacological potential of a molecule. As shown in Figure 9a, the curcumin-AKT1 complex maintained a uniform Rg pattern with a minor increase and decrease behavior between 60 and 80 ns; however, subsequently, it stabilized and maintained a steady level of 17.10 Å during the latter part of the simulation. Similarly, the Rg pattern for the curcumin-TNF-α complex started from 20.0 Å and reached the maximum (20.40 Å) at 10 ns and then decreased back. The Rg maintained a stable level throughout the simulation. An average Rg for the curcumin-TNF-α complex was calculated to be 20.10 Å and is presented in Figure 9b. The curcumin-EGFR complex also reported a uniform pattern of Rg with no variation during the simulation. The Rg though increased at 120 ns it then decreased back and stabilized at an average Rg value of 20.75 Å. The Rg graph for the curcumin-EGFR is shown in Figure 9c. The Rg of the curcumin-STAT3 complex started to increase gradually, and this pattern was observed between 1–70 ns; however, the Rg values then decreased and stabilized at 14.20 Å with no significant perturbation in the pattern. The Rg graph for the curcumin-STAT3 is shown in Figure 9d. Overall, the current findings demonstrate that minimal unbinding events were observed and the Rg remained uniform for all the complexes during most of the simulation time. These observations further underscore the pharmacological potential of curcumin in binding to AKT1, TNF-α, EGFR, and STAT3.

3.8. Residue's Flexibility Analysis

In molecular dynamics simulations, the RMSF serves as a valuable metric for assessing the flexibility of various regions within

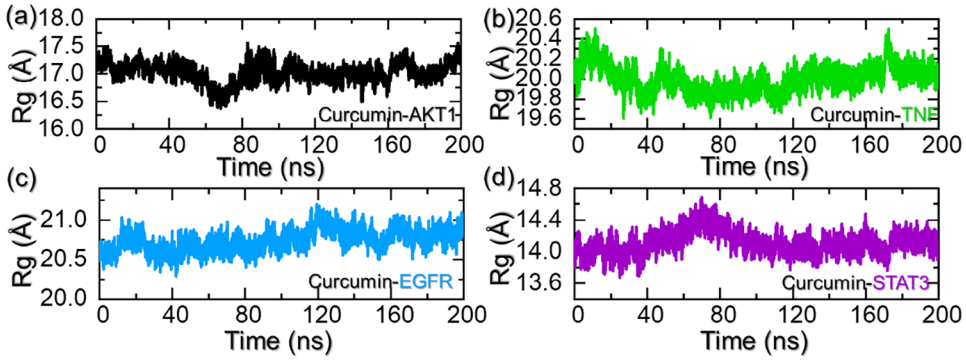

Figure 9. Structural compactness analysis of the curcumin-bound complexes. Panel (a) shows the Rg graph for curcumin-AKT1 complex, panel (b) shows the Rg graph for the curcumin-TNF-α complex, panel (c) shows the Rg graph for the curcumin-EGFR while panel (d) shows the Rg graph for the curcumin-STAT3 complex.

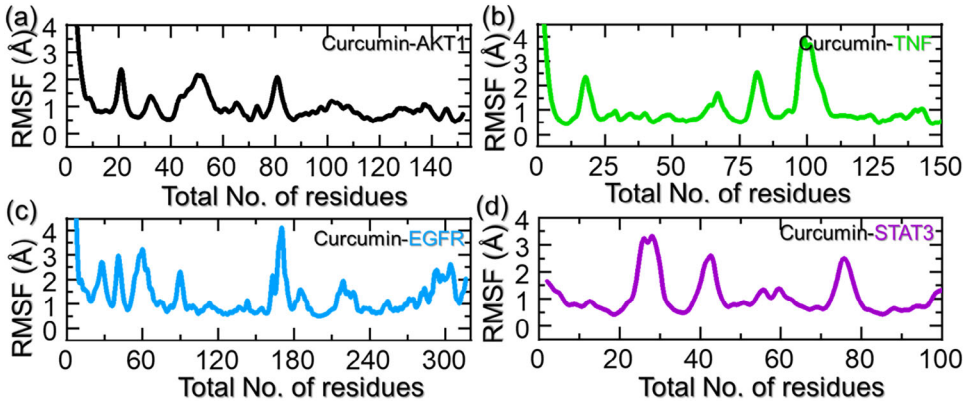

Figure 10. Residue's flexibility analysis of the curcumin-bound complexes. Panel (a) shows the RMSF graph for the curcumin-AKT1 complex, panel (b) shows the RMSF graph for the curcumin-TNF-α complex, panel (c) shows the RMSF graph for the curcumin-EGFR while panel (d) shows the RMSF graph for the curcumin-STAT3 complex.

a molecule or across different molecules. This assessment can pinpoint flexible regions that are potentially crucial for ligand binding or protein-protein interactions (PPIs). Additionally, RMSF is a critical parameter for validating molecular dynamics simulations. By comparing experimental RMSF measurements with simulated values, researchers can evaluate the accuracy of the simulation and the force field employed. A strong correlation between experimental and simulated RMSF values suggests that the simulation effectively captures the biomolecule's flexibility and dynamics. In the case of curcumin-AKT1 complex, the region between 20–90 demonstrated higher flexibility while the other regions reported minimal fluctuations. The binding of curcumin occurs at 100–150 residues and thus stabilizes the internal fluctuation upon the binding. The RMSF graph for curcumin-AKT1 complex is provided in Figure 10a. We also evaluated the flexibility of the curcumin-TNF-α complex, which reported that regions 15–25, 75–85, and 97–112 had higher fluctuations than the rest of the structure. The RMSF graph for curcumin-TNF-α complex is given in Figure 10b. In the case of curcumin-EGFR, a higher fluctuation was observed for the regions between 10–70 and 160–180 amino acids. While the curcumin-STAT3 reported mostly higher fluctuations for most of the protein regions. The RMSF graphs for the curcumin-EGFR and curcumin-STAT3 complexes are given in Figure 10c,d. In certain regions, the increased flexibility or dynamic motion, suggests that the binding of the ligand induces structural changes or instability in those specific areas. On the other hand, lower RMSF in certain regions suggests stabilization or reduced flexibility due to the ligand binding.

3.9. Binding Free Energy Calculation

To validate the docking outcomes, one can employ the binding free energy calculation method, known for its accuracy, speed, and computational efficiency. This widely utilized approach has proven effective in assessing the binding potential of diverse protein complexes implicated in various diseases. Hence, acknowledging the efficacy of this method, we conducted binding free energy calculations utilizing the MM/GBSA and MM/PBSA methods. As summarized in Tables 2 and 3, the vdW values calculated using the MM/GBSA method were -39.73 ± 0.23 kcal/mol for curcumin-AKT complex, -23.98 ± 0.41 kcal/mol for the curcumin-TNF-α complex, -30.58 ± 0.15 for the curcumin-EGFR complex, and -39.15 ± 0.16 kcal/mol for the curcumin-STAT3 complex. The electrostatic energy was also calculated for each complex and showed values of -7.94 ± 0.28 for the Curcumin-AKT complex, -1.49 ± 0.10 kcal/mol for the curcumin-TNF-α

Table 2. Binding free energy calculation using the MM/GBSA method. The results are expressed in kcal/mol.

Parameters	Curcumin-AKT1	Curcumin- TNF-α	Curcumin-EGFR	Curcumin-STAT3
VDWAALS	−39.73 ± 0.23	−23.98 ± 0.41	−30.58 ± 0.15	−39.15 ± 0.16
EEL	−7.94 ± 0.28	−1.49 ± 0.10	−9.04 ± 0.16	−14.51 ± 0.22
EGB	21.29 ± 0.27	6.91 ± 0.14	19.48 ± 0.18	27.45 ± 0.23
ESURF	−4.55 ± 0.01	−2.80 ± 0.03	−3.28 ± 0.01	−4.33 ± 0.01
DELTA G gas	−47.68 ± 0.33	−25.47 ± 0.47	−37.63 ± 0.25	−53.66 ± 0.31
DELTA G solv	16.73 ± 0.26	4.11 ± 0.11	16.19 ± 0.18	23.11 ± 0.23
DELTA TOTAL	**−30.94 ± 0.21**	**−21.35 ± 0.38**	**−23.43 ± 0.13**	**−30.54 ± 0.19**

Table 3. Binding free energy calculation using the MM/PBSA methods. The results are expressed in kcal/mol.

Parameters	Curcumin-AKT1	Curcumin- TNF-α	Curcumin-EGFR	Curcumin-STAT3
VDWAALS	−39.73 ± 0.23	−23.98 ± 0.41	−28.58 ± 0.15	−39.15 ± 0.16
EEL	−7.94 ± 0.28	−1.49 ± 0.10	−9.04 ± 0.16	−14.51 ± 0.22
EPB	24.25 ± 0.34	7.84 ± 0.19	17.92 ± 0.20	32.41 ± 0.26
ENPOLAR	−3.23 ± 0.01	−2.18 ± 0.02	−2.72 ± 0.01	−3.01 ± 0.00
DELTA G gas	−47.68 ± 0.33	−25.47 ± 0.47	−37.63 ± 0.25	−53.66 ± 0.31
DELTA G solv	21.01 ± 0.34	5.66 ± 0.17	15.19 ± 0.19	29.39 ± 0.25
DELTA TOTAL	**−26.66 ± 0.24**	**−19.80 ± 0.32**	**−22.43 ± 0.14**	**−24.27 ± 0.22**

complex, −9.04 ± 0.16 for the curcumin-EGFR complex, and −14.51 ± 0.22 kcal/mol for the curcumin-STAT3 complex. The total binding free energy for each of these complexes was also calculated using to MM/GBSA and showed values of −30.94 ± 0.21 kcal/mol for the curcumin-AKT1 complex, −21.35 ± 0.38 kcal/mol for the curcumin-TNF-α complex, −23.43 ± 0.13 kcal/mol for the curcumin-EGFR complex, and −30.54 ± 0.19 kcal/mol for the curcumin-STAT3 complex. This shows a more robust binding of curcumin to these receptors in diabetes and consequently produces better pharmacological properties.

On the other hand, the total binding free energy for each complex calculated using the MM/PBSA method showed values of −26.66 ± 0.24 kcal/mol for the curcumin-AKT1 complex, −19.80 ± 0.32 kcal/mol for the curcumin-TNF-α complex, −22.43 ± 0.14 kcal/mol for the curcumin-EGFR complex, and −24.27 ± 0.22 kcal/mol for the curcumin-STAT3 complex. The MM/PBSA results are summarized in Table 3. Analysis of the data reveals that each system experiences an increase in free energy in the gas phase but not in the solvent state. These results imply that the thermodynamic preference for curcumin binding is primarily dictated by enthalpic factors, with favorable interactions dominating in the gas phase. Conversely, the binding is unfavorable in terms of entropy, attributed to the adverse effects of solvation.

4. Conclusions

The current study employs network pharmacology and molecular simulation-based approaches to identify potential targets for curcumin in diabetes. Among the identified hits, only four targets, i.e., AKT1, TNF-α, EGFR, and STAT3 were reported as the key hub genes that could act as key biomarkers. Using the QPLD approach, we revealed robust interactions and key pathways that are regulated by these genes. Moreover, molecular simulation results demonstrated stable dynamic behavior, compact structure, and differences in the residue's flexibility. The binding free energy results further re-evaluated the docking complexes and reported that each system experiences an increase in free energy in the gas phase but not in the solvent. These results imply that the thermodynamic preference for curcumin binding is primarily dictated by enthalpic factors, with favorable interactions dominating in the gas phase. Conversely, the binding is unfavorable in terms of entropy, attributed to the adverse effects of solvation. Altogether, the findings of our study provide valuable insight into the molecular targets of curcumin in diabetes and establish a foundation for future progress in diabetes treatment by underscoring the importance of these hub genes in the pathogenesis of diabetes.

Acknowledgements

This work was supported by Qatar University grant No. QUPD-CPH-23/24-592. M.A.Z. is supported by Ph.D. graduate assistantships from the Office of Graduate Studies (Qatar University). The statements made herein are solely the responsibility of the authors.

Conflict of Interests

The authors declare no conflict of interest.

Data Availability Statement

The data that support the findings of this study are available from the corresponding author upon reasonable request.

Keywords: Binding free energy · Curcumin · Diabetes · Molecular docking simulation · Network pharmacology

[1] M. S. Kumari, M. K. Babu, M. R. Sulthana, M. Srinivas, C. Prasanthi, *Insulin* **2014**, *2*, 18–24.
[2] Z. Fu, R E. Gilbert, D. Liu, *Curr. Diabetes Rev.* **2013**, *9*, 25–53.
[3] M. Dwivedi, A. R. Pandey, *J. Adv. Pharmacol.* **2020**, *1*, 48–58.
[4] D. Lovic, A. Piperidou, I. Zografou, H. Grassos, A. Pittaras, A. Manolis, *Curr. Vasc. Pharmacol.* **2020**, *18*, 104–109.
[5] P. Saeedi, I. Petersohn, P. Salpea, B. Malanda, S. Karuranga, N. Unwin, S. Colagiuri, L. Guariguata, A. A. Motala, K. Ogurtsova, *Diabetes Res. Clin. Pr.* **2019**, *157*, 107843.
[6] P. Arokiasamy, S. Salvi, Y. Selvamani, *Handbook of Global Health* **2021**, 495–538.
[7] L. A. Paul, M. S. Garba, D. A. Dangiwa, M. Dayol, *J Clin. Pharm. Ther.* **2023**, *2*. https://njcpt.com.ng/101.1.2.26.
[8] P. Tiwari, *J. Diabetes Res.* **2015**, *2015*, 1-11.
[9] C. Roumen, E. E. Blaak, E. Corpeleijn, *Nutr. Rev.* **2009**, *67*, 132–146.
[10] M. Gillett, P. Royle, A. Snaith, G. Scotland, A. Poobalan, M. Imamura, C. Black, M. Boroujerdi, S. Jick, L. Wyness, *Health technology assessment* **2012**, *16*.
[11] S. Chinenye, A. E. Uloko, A. O. Ogbera, E. N. Ofoegbu, O. A. Fasanmade, A. A. Fasanmade, O. O. Ogbu, *Indian J. Endocrinol. Metab.* **2012**, *16*, 558.
[12] A. Paul, M. Kumar, P. Das, N. Guha, M. Rudrapal, M. K. Zaman, *Biomed. Pharmacother.* **2022**, *156*, 113846.
[13] H. Ye, J. Wei, K. Tang, R. Feuers, H. Hong, *Curr. Top. Med. Chem.* **2016**, *16*, 3646–3656.
[14] U. Chandran, N. Mehendale, S. Patil, R. Chaguturu, B. Patwardhan, *Innovative Approaches in Drug Discovery* **2017**, 127.
[15] M. Kibble, N. Saarinen, J. Tang, K. Wennerberg, S. Mäkelä, T. Aittokallio, *Nat. Prod. Rep.* **2015**, *32*, 1249–1266.
[16] B. Meng, J. Li, H. Cao, *Curr. Pharm. Des.* **2013**, *19*, 2101–2113.
[17] Z.-h. Xia, S.-y. Zhang, Y.-s. Chen., K. Li, W.-b. Chen, Y.-q. Liu, *Food Chem. Toxicol.* **2020**, *146*, 111803.
[18] J. S. Bhatti, A. Sehrawat, J. Mishra, I. S. Sidhu, U. Navik, N. Khullar, S. Kumar, G. K. Bhatti, P. H. Reddy, *Free Radic. Biol. Med.* **2022**, *184*, 114–134.
[19] X. Nie, Z. Chen, L. Pang, L. Wang, H. Jiang, Y. Chen, Z. Zhang, C. Fu, B. Ren, J. Zhang, *Int. J. Nanomed.* **2020**, 10215–10240.
[20] A. Daina, O. Michielin, V. Zoete, *Nucleic Acids Res.* **2019**, *47*, W357-W364.
[21] K. Gallo, A. Goede, R. Preissner, B.-O. Gohlke, *Nucleic Acids Res.* **2022**, *50*, W726-W731.
[22] D. Szklarczyk, A. L. Gable, K. C. Nastou, D. Lyon, R. Kirsch, S. Pyysalo, N. T. Doncheva, M. Legeay, T. Fang, P. Bork, *Nucleic Acids Res.* **2021**, *49*, D605-D612.
[23] N. T. Doncheva, J. H. Morris, H. Holze, R. Kirsch, K. C. Nastou, Y. Cuesta-Astroz, T. Rattei, D. Szklarczyk, C. von Mering, L. J. Jensen, *J. Proteome Res.* **2022**, *22*, 637–646.
[24] D. Otasek, J. H. Morris, J. Bouças, A. R. Pico, B. Demchak, *Genome Biol.* **2019**, *20*, 1–15.
[25] S. Lotia, J. Montojo, Y. Dong, G. D. Bader, A. R. Pico, *Bioinformatics* **2013**, *29*, 1350–1351.
[26] C.-H. Chin, S.-H. Chen, H.-H. Wu, C.-W. Ho, M.-T. Ko, C.-Y. Lin, **2014**, *BMC Syst. Biol. 8*, 1–7.
[27] J. Jumper, R. Evans, A. Pritzel, T. Green, M. Figurnov, O. Ronneberger, K. Tunyasuvunakool, R. Bates, A. Žídek, A. Potapenko, *Nature* **2021**, *596*, 583–589.
[28] S. K. Burley, H. M. Berman, C. Bhikadiya, C. Bi, L. Chen, L. Di Costanzo, C. Christie, K. Dalenberg, J. M. Duarte, S. Dutta, *Nucleic Acids Rese.* **2019**, *47*, D464-D474.
[29] S. Maestro, Maestro. Schrödinger, LLC, New York, NY **2020**, *2020*.
[30] L. G. Ferreira, Dos R. N. Santos, G. Oliva, A. D. Andricopulo, *Molecules (Basel, Switzerland)* **2015**, *20*, 13384-13421.
[31] A. E. Cho, V. Guallar, B. J. Berne, R. Friesner, *J. Comput. Chem.* **2005**, *26*, 915–931.
[32] W. L. DeLano, *CCP4 Newsletter on Protein Crystallography* **2002**, *40*, 82–92.
[33] D. A. Case, E. T. Cheatham III, T. Darden, H. Gohlke, R. Luo, K. M. Merz Jr., A. Onufriev, C. Simmerling, B. Wang, R. J. Woods, *J. Comput. Chem.* **2005**, *26*, 1668–1688.
[34] R. Salomon-Ferrer, D. A. Case, R. C. Walker, *Wiley Interdiscip Rev Comput Mol Sci* **2013**, *3*, 198–210.
[35] A. Toukmaji, C. Sagui, J. Board, T. Darden, *J. Chem. Phys.* **2000**, *113*, 10913–10927.
[36] M. Fyta, In *Computational Approaches in Physics*, Morgan & Claypool Publishers, Bristol, United Kingdom, **2016**.
[37] R. Salomon-Ferrer, A. W. Gotz, D. Poole, S. Le Grand, R. C. Walker, *J. Chem. Theory Comput.* **2013**, *9*, 3878–3888.
[38] D. R. Roe, E. T. Cheatham III, *J. Chem. Theory Comput.* **2013**, *9*, 3084–3095.
[39] V. N. Maiorov, G. M. Crippen, *J. Mol. Biol.* **1994**, *235*, 625–634.
[40] A. Cooper, *Proc. Natl. Acad. Sci. USA* **1976**, *73*, 2740–2741.
[41] M. Y. Lobanov, N. Bogatyreva, O. Galzitskaya, *Molecular Biology* **2008**, *42*,, 623–628.
[42] F. Chen, H. Liu, H. Sun, P. Pan, Y. Li, D. Li, T. Hou, *Phys. Chem. Chem. Phys.* **2016**, *18*, 22129–22139.
[43] S. Nadeem, S. Akhtar, A. Saleem, N. Akkurt, H. A. Ghazwani, S. M. Eldin, *Alexandria Eng. J.* **2023**, *69*, 613–637.
[44] I. Chattopadhyay, K. Biswas, U. Bandyopadhyay, R. K. Banerjee, *Current Science* **2004**, pp. 44–53.
[45] P. Tresina, M. S. Selvam, A. Doss, V. Mohan, *Stud. Nat. Prod. Chem.* **2022**, *75*, 75–118.
[46] N. Safari-Alighiarloo, M. Taghizadeh, M. Rezaei-Tavirani, B. Goliaei, A. A. Peyvandi, *Gastroenterol. Hepatol. Bed Bench.* **2014**, *7*, 17.
[47] A. Khan, Z. Rehman, H. F. Hashmi, A. A. Khan, M. Junaid, A. M. Sayaf, S. S. Ali, F. U. Hassan, W. Heng, D.-Q. Wei, *Interdiscip. Sci.* **2020**, *12*, 155–168.
[48] G. Selvaraj, S. Kaliamurthi, A. C. Kaushik, A. Khan, Y.-K. Wei, W. C. Cho, K. Gu, D.-Q. Wei, *J. Biomed. Inform.* **2018**, *86*, 120–134.
[49] X. Huang, G. Liu, J. Guo, Z. Su, *Int. J. Biol. Sci.* **2018**, *14*, 1483–1496.
[50] I. Camaya, S. Donnelly, B. O'Brien, *J. Diabetes* **2022**, *14*, 247–260.
[51] R. Miao, X. Fang, J. Wei, H. Wu, X. Wang, J. Tian, *Front. Physiol.* **2022**, *13*.
[52] M. S. H. Akash, K. Rehman, A. Liaqat, *J. Cell. Biochem.* **2018**, *119*, 105–110.
[53] B. Ke, Z. Zhao, X. Ye, Z. Gao, V. Manganiello, B. Wu, J. Ye, *Diabetes* **2015**, *64*, 3355-3362.
[54] N. W. Zammit, Y. Y. Wong, S. N. Walters, J. Warren, S. C. Barry, S. T. Grey, *Diabetologia* **2023**, *66*, 1516–1531.
[55] T. Gregg, S. M. Sdao, R. S. Dhillon, J. W. Rensvold, S. L. Lewandowski, D. J. Pagliarini, J. M. Denu, M. J. Merrins, *J. Biol. Chem.* **2019**, *294*, 4656–4666.
[56] J. R. Ow, M. J. Caldez, G. Zafer, J. C. Foo, H. Y. Li, S. Ghosh, H. Wollmann, A. Cazenave-Gassiot, C. B. Ong, M. R. Wenk, W. Han, H. Choi, P. Kaldis, *eLife* **2020**, *9*, e63835.
[57] A. Subramanian, P. Tamayo, V. K. Mootha, S. Mukherjee, B. L. Ebert, M. A. Gillette, A. Paulovich, S. L. Pomeroy, T. R. Golub, E. S. Lander, *Proc. Natl. Acad. Sci. USA* **2005**, *102*, 15545–15550.
[58] M. F. El-Azab, F. M. Attia, A. M. El-Mowafy, *Eur. J. Pharmacol.* **2011**, *658*, 41–48.
[59] M. A. El-Moselhy, A. Taye, S. S. Sharkawi, S. F. I. El-Sisi, A. F. Ahmed, *Food Chem. Toxicol.* **2011**, *49*, 1129–1140.

Manuscript received: May 16, 2024